H_0 tension or T_0 tension?

Mikhail M. Ivanov,[1,2,][*] Yacine Ali-Haïmoud,[1,][†] and Julien Lesgourgues[3,][‡]

[1]*Center for Cosmology and Particle Physics, Department of Physics,*
New York University, New York, NY 10003, USA
[2]*Institute for Nuclear Research of the Russian Academy of Sciences,*
60th October Anniversary Prospect, 7a, 117312 Moscow, Russia
[3]*Institute for Theoretical Particle Physics and Cosmology (TTK)*
RWTH Aachen University, D-52056 Aachen, Germany

We study whether the discrepancy between the local and cosmological measurements of the Hubble constant H_0 can be reformulated as a tension in the cosmic microwave background (CMB) monopole temperature T_0. The latter is customarily fixed to the COBE/FIRAS best-fit value in CMB anisotropy data analyses. We show that the primary CMB anisotropies and the shape of the matter power spectrum are not directly sensitive to T_0. They depend only on the dark matter and baryon densities per CMB photon. Once these ratios are fixed, T_0 only measures the time elapsed since recombination until today. This results is a nearly perfect geometric degeneracy between T_0 and H_0. Taken at face value, this implies that removing the FIRAS prior on T_0 is enough to make the Planck CMB and SH0ES measurements consistent within the base ΛCDM model without introducing new physics. One may break the degeneracy by combining Planck with SH0ES, yielding an independent measurement of T_0, which happens to be in a 4σ tension with FIRAS. Therefore, the Hubble tension can be fully recast into the T_0 tension. The agreement with FIRAS can be restored if we combine Planck with the baryon acoustic oscillation data instead of SH0ES. Thus, the tension between SH0ES and cosmological measurements of H_0 within ΛCDM persists even if we discard the FIRAS T_0 measurement.

1. INTRODUCTION AND SUMMARY

The disagreement between the value of the Hubble constant H_0 measured by different methods (the so-called "Hubble tension") has recently become a hot topic in cosmology. On the one hand, local measurements using the Cepheid-calibrated supernovae [1, 2] and strong lensing time-delays [3] yield a number around 74 km/s/Mpc. On the other hand, the Planck cosmic microwave background radiation (CMB) data [4], various large-scale structure (LSS) probes [5–11], as well as the local measurements based on the inverse distance ladder technique [12, 13] favour independently of each other a value close to 68 km/s/Mpc. The Hubble tension might be the result of unaccounted systematics[1] or a manifestation of new exotic physics (see Ref. [17] for a review). Therefore, it is

imperative to scrutinize various choices made in the analysis of each dataset. One of such assumptions is the value of the CMB monopole temperature T_0, which is typically fixed when fitting the Planck CMB likelihoods. The rationale behind this choice is that T_0 has been measured from a combination of the COBE/FIRAS data, molecular lines, and balloon-borne experiments with an outstanding precision [18, 19],[2]

$$T_{0,\text{FIRAS}} = (2.72548 \pm 0.00057) \text{ K} . \tag{1}$$

The effect of T_0 on CMB anisotropies was studied in Refs. [20–24]. These past studies have either focused on the impact of uncertainties in T_0 on cosmological parameters inferred from CMB anisotropy data [20–22], on combining current CMB anisotropy data with external datasets to measure T_0 [23], or on determining whether future CMB-anisotropy experiments might be able to measure T_0 [24]. In this paper, we show, for the first time, that T_0 can be measured from *current* CMB anisotropy

---

[*] mi1271@nyu.edu

[†] yah2@nyu.edu

[‡] julien.lesgourgues@physik.rwth-aachen.de

[1] See, e.g. Ref. [14] in the context of the Cepheid-calibrated supernovae and Refs. [15, 16] for discussions regarding the strong lensing time delays.

[2] For simplicity, we will call this measurement just "FIRAS."

data *alone*. We moreover study whether removing the FIRAS prior on T_0 can alleviate the Hubble tension. Since the monopole temperature can be seen as a proxy for the age of the Universe, just like H_0, the two quantities should be nearly perfectly degenerate. Clearly, the CMB measurement of H_0 must be influenced by the T_0 prior. Naively, this offers a tempting way to resolve the Hubble tension without new physics and any additional parameters beyond those already contained in the base ΛCDM model.

Aiming at restoring the agreement between Planck and SH0ES, we have reanalyzed the final Planck 2018 data without fixing the CMB monopole temperature. As expected, we have found that the CMB data exhibit a clear H_0-T_0 degeneracy. This significantly loosens the bounds on H_0, which, at face value, becomes compatible with the SH0ES measurement. Thus, combining Planck and SH0ES gives an *independent measurement* of T_0. This value happens to be in $\sim 4\sigma$ tension with the FIRAS measurement. However, one can break the geometric CMB degeneracy between T_0 and H_0 equally well with low-redshift baryon acoustic oscillation (BAO) data. This leads to a different measurement of T_0 that agrees with FIRAS, while being in $\sim 4\sigma$ tension with SH0ES.

Thus, interestingly, the Hubble tension between Planck+FIRAS and SH0ES can be fully reformulated as a T_0 tension between Planck+SH0ES and FIRAS. However, when BAO data is taken into account, the very good agreement between the measurements of Planck, FIRAS and BAO suggests that, as long as the ΛCDM model is assumed, SH0ES is the outlier.

Another goal of this paper is to clarify the physical effect of T_0 on cosmological observables. In past works [20, 21], T_0 was varied while keeping H_0 and the *current* energy densities of the baryons and dark matter ω_b and ω_{cdm} fixed. However, recombination physics and the early-time CMB anisotropies are fully determined by the baryon-to-photon and CDM-particles-to-photon ratios, which results in almost perfect degeneracies between $H_0, \omega_b, \omega_{cdm}$ and T_0 [24]. Thus, varying T_0 with fixed H_0, ω_{cdm} and ω_b is not very informative. Instead, we show that it is more physically meaningful to study the effect of T_0 while keeping the ratios ω_{cdm}/T_0^3 and ω_b/T_0^3 constant. With these parameters fixed, the *temperature* of recombination is fixed, and a change of T_0 *mostly* amounts to changing the angular diameter distance to the last scattering surface, thus the angle θ_s that

it substends, resulting in a strong degeneracy with H_0. In addition, however, a change in T_0 at fixed θ_s changes the time elapsed since matter-Λ equality, thus the late integrated Sachs-Wolfe effect and gravitational lensing. Through these late-time effects, we show that one can extract a 2% measurement of T_0 from Planck data *alone*, contrasting with the standard lore that this could not be done without external datasets[3] [23, 24].

The remainder of this paper is structured as follows. We start with the discussion of our datasets in Sec. 2. We give some theoretical background in Sec. 3, whereas Sec. 4 contains our main results. Finally, we draw conclusions in Sec. 5.

2. DATA

For CMB anisotropy data, we use the Planck baseline TTTEEE + low ℓ + lensing likelihood from the 2018 data release [4] as implemented in `Montepython v3.0` [25], see Ref. [26] for likelihood details. Since the standard recombination code `recfast` [27] uses fudge functions calibrated for a fixed T_0, we use the more flexible and accurate code `HyRec` [28, 29] that does not rely on any fiducial cosmology. In addition to the cosmological parameters, we vary 21 Planck nuisance parameters that capture various instrumental and systematic effects [26].

As for the SH0ES data, we will use a Gaussian prior on H_0 derived from the most recent measurements by the SH0ES collaboration [2],

$$H_0 = 73.5 \pm 1.4 \quad \text{km/s/Mpc}. \qquad (2)$$

Moreover, we will employ BAO data from the BOSS data release 12 [30]. In principle, one can derive better constraints from the full BOSS likelihood that includes the shape information as well [31]. However, the compressed likelihood involving only the BAO scale will be sufficient if our goal is to break geometric degeneracies (see Ref. [32] for a discussion on the role of the BOSS data in combination with Planck). In principle, one can also use more BAO measurements, e.g. from the Ly-α [33] and quasar data [34]. However, the single most constraining BAO dataset from BOSS DR12 will be enough for the purposes of our paper.

----

[3] Of course, an external dataset (the FIRAS dipole) is required for the absolute calibration of Planck.

The CMB monopole temperature T_0 has already been constrained independently of FIRAS in the Planck 2015 analysis [23], which gave the following result from the combination of TT, TE, EE and BAO data,

$$T_0 = (2.718 \pm 0.021) \text{ K} . \tag{3}$$

In this paper, it was already pointed out that the Planck data have a strong geometric degeneracy between H_0 and T_0, which can be broken by BAO measurements. In the next sections we will explain in detail the origin of this degeneracy, and show how it can also be broken by SH0ES.

3. THEORY BACKGROUND

3.1. Cosmological model and parameters

In this paper, we use geometric units $G = c = 1$. For short, we define the constant rate

$$\gamma_{100} \equiv \frac{H_0}{h} = 100 \text{ km/s/Mpc}. \tag{4}$$

In what follows we will focus on the Planck baseline ΛCDM model [4]. Specifically, we assume a spatially flat Universe with a cosmological constant $\Lambda = 8\pi\rho_\Lambda$, containing thermal photons at temperature T_γ, cold dark matter, non-relativistic baryons, two massless neutrinos and a single massive neutrino with minimal mass $m_\nu = 0.06$ eV (but our entire discussion would hold in the more realistic case of three non-zero masses). We assume that neutrinos have the standard temperature $T_\nu = (4/11)^{1/3}T_\gamma$, and that the small non-thermal distortions to their spectrum can be accounted for with an effective number of relativistic degrees of freedom $N_{\text{eff}} = 3.046$.

Moreover, we assume scalar adiabatic initial conditions characterized by a simple power-law power spectrum. The cosmological model is then entirely determined by 7 parameters:

• 2 parameters determining the initial conditions: the amplitude A_s at a reference scale $k_P = 0.05$ Mpc^{-1} and tilt n_s of the spectrum of primordial curvature fluctuations $\mathcal{R}$, $\Delta_\mathcal{R}^2 = A_s(k/k_P)^{n_s-1}$.

• 4 independent parameters determining the matter and energy content: the cosmological constant Λ, the present-time radiation temperature T_0 and the present-time baryon and cold dark matter densities $\rho_{b,0}, \rho_{c,0}$, or their dimensionless versions $\omega_i \equiv \frac{8\pi}{3}\rho_{i,0}/\gamma_{100}^2$. Instead of

Λ, one can equivalently use the Hubble parameter H_0 or the angular scale θ_s of the sound horizon at last scattering. This phenomenological parameter is designed to approximate the observed angular scale of the CMB acoustic peaks.[4]

• 1 astrophysical parameter: the optical depth τ_{reio} to reionization.

3.2. How can we know whether T_0 is measurable?

It is standard in CMB anisotropy analyses to set T_0 to the mean value measured by FIRAS. Here we shall instead take T_0 as a free parameter. To check whether T_0 is actually measurable, we want to understand whether the impact of a variation of T_0 on cosmological observables can be absorbed by a rescaling of other parameters. Such observables depend on the evolution of several quantities that can be expressed as a function of different measures of time: proper time t, conformal time η, redshift z, the scale factor $a = 1/(1+z)$, the energy scale, etc. We want to study whether we can "vary T_0 and other parameters while keeping the cosmological evolution unchanged", but given the previous remark, this could have several different meanings. The most relevant options are:

(i) To maintain a fixed expansion history *relative to today*. This choice may also be sensible, because several observables depend on characteristic scales measured relatively to lengths today, and on the amount of expansion between characteristic times and today. For instance, the amplitude of matter perturbations at some redshift z relative to their amplitude today depends on the value of their wavelength relative to the Hubble radius today; the angle under which we see features in correlation functions depends on their size relative to the angular diameter distance, that we compute by integrating the expansion history relatively to the present time; the late integrated Sachs-Wolfe effect depends on the amount of expansion between matter-to-Λ equality

---

[4] By definition $\theta_s = r_s/((1 + z_*)D_A(z_*))$ (r_s is the comoving sound horizon at the redshift of recombination z_*, $D_A(z_*)$ is the angular diameter distance to the last scattering surface). It should be borne in mind that this definition is somewhat ambiguous because recombination is not an instantaneous process.

and today; etc. To explore such a degeneracy, we should try to express all relevant quantities as a function of the redshift z (i.e. of the scale factor relative to today), and to show that if cosmological parameters are scaled properly when T_0 is varied, the quantities over which cosmological observables depend remain invariant. This could be achieved to some extent by fixing the parameter combinations ω_b/T_0^4, ω_{cdm}/T_0^4, Λ/T_0^4, $N_{\rm eff}$, etc.

(ii) To maintain cosmological evolution (of background, thermodynamics and perturbed quantities) as a function of *absolute energy scales*. This choice is motivated by the fact that important phenomena like nucleosynthesis or recombination are determined by absolute energy scales, such as particle masses, nuclear and atomic binding energies and energy levels, the neutron lifetime, etc. The most natural way to parametrize the energy scale is through the temperature of the thermal bath, T_γ. In this case, as we will see shortly, it is more meaningful to parametrize the baryon and dark matter densities by the following parameters, which are proportional to the time-independent baryon-to-photon and dark matter-to-photon *number ratios*:

$$\varpi_i \equiv \frac{\omega_i}{T_0^3}, \quad i = b, c. \tag{5}$$

We also define $\varpi_m \equiv \varpi_b + \varpi_{cdm}$. As we will see, all cosmological quantities *at a given T_γ* depend on the parameters $\varpi_i, \Lambda, N_{\rm eff}$, etc., but not *directly* on T_0. This parametrization of the evolution of the Universe also requires redefining "comoving" scales as physical scales at a fixed *energy scale*, rather than a fixed *time*.

Of course, cosmological observables depend *both* on absolute energy scales and on the expansion history relative to today. Since the two scalings described above are incompatible with each other, a variation of T_0 cannot be fully absorbed. Thus the present photon temperature is indeed measurable with cosmological data, independently of FIRAS.

3.3. Background evolution and last scattering

We now show that, when expressing background quantities in terms of the photon temperature (rather than time t, redshift z or scale factor a), following the second scaling described in the previous section, they do not depend on T_0, at fixed baryon-to-photon and CDM-to-photon number ratios ϖ_b, ϖ_{cdm}.

First, the Hubble rate $H(T_\gamma)$ is given by

$$H^2(T_\gamma) = \frac{\Lambda}{3} + \gamma_{100}^2 \left(\mathcal{A}(T_\gamma) \, T_\gamma^4 + \varpi_m T_\gamma^3 \right), \tag{6}$$

where the function $\mathcal{A}(T_\gamma)$ is equal to a fixed number $\bar{\mathcal{A}}$ proportional to $1 + \frac{7}{8} \left(\frac{4}{11} \right)^{4/3} N_{\rm eff}$ until the heaviest neutrino becomes non-relativistic, and later on only depends on the ratio[5] m_ν/T_γ. Thus matter-radiation equality occurs at a temperature $T_{\rm eq} = \varpi_m/\bar{\mathcal{A}}$ that only depends on ϖ_m. Of course, the *current* Hubble rate H_0 does depend on the current CMB temperature T_0. Thus one can think of T_0 as parametrizing the current age of the Universe.

Second, in our baseline ΛCDM model, primordial nucleosynthesis starts with deuterium fusion, at a temperature fixed by the baryon-to-photon number ratio and the deuterium binding energy. The final abundance of all primordial nuclei depends on nuclear rates and on the neutron-to-proton ratio, governed by the neutron lifetime, the effective number of degrees of freedom of the Standard Model, and the Fermi constant. Thus, in the minimal cosmological model, the only cosmological parameter relevant for this process is the baryon-to-photon number ratio, or equivalently ϖ_b. It sets in particular the primordial Helium fraction, $Y_{\rm He}$, which is relevant for cosmological recombination.

Lastly, cosmological recombination can formally be described by coupled equations of the form (see, e.g. [29])

$$\frac{dx_e}{dt} = \mathcal{F}(x_e, T_e, f_\nu, \rho_b, H, T_\gamma), \tag{7}$$

$$\frac{dT_e}{dt} = \mathcal{G}(x_e, T_e, H, T_\gamma), \tag{8}$$

$$\frac{df_\nu}{dt} = \mathcal{C}(x_e, f_\nu, \rho_b, H, T_\gamma), \tag{9}$$

where x_e is the free electron fraction, T_e is the electron temperature, f_ν is the photon phase-space density in the neighborhood of the Lyman-α transition, and the last equation is a Boltzmann equation describing its evolution. Upon rewriting these equations in terms of $dx_e/dT_\gamma, dT_e/dT_\gamma, df_\nu/dT_\gamma$, and using the fact that

———

[5] or more realistically on $\sum_i m_{\nu i}/T_\gamma$, where the sum runs over all neutrinos that are non-relativistic at a given time.

$\rho_b \propto \varpi_b T_\gamma^3$ and H is a function of ϖ_m and T_γ only at the recombination epoch, we find that the free-electron fraction is a function of T_γ and ϖ_b, ϖ_{cdm} only:

$$x_e = x_e(T_\gamma; \varpi_b, \varpi_{cdm}). \tag{10}$$

We show the free-electron fraction for different values of T_0 in Fig. 1, where we illustrate that, when keeping constant baryon-to-photon and dark matter-to-photon number ratios and expressing x_e as a function of T_γ, it is indeed independent of T_0.

Given the recombination history $x_e(T_\gamma)$, one can compute the visibility function $g(\eta)$, which is the differential probability of last scattering per unit conformal time η:

$$g(\eta) \equiv \dot{\tau} \exp\left[-\int_\eta^{\eta_0} d\eta' \dot{\tau}(\eta')\right] \tag{11}$$

where $\dot{\tau} = a n_H x_e \sigma_T$ is the differential Thomson optical depth, and η_0 is the current conformal time. It peaks at η_* such that $g'(\eta_*) = 0$, which thus solves the equation

$$\left.\frac{d\dot{\tau}}{d\eta}\right|_{\eta_*} = \dot{\tau}^2(\eta_*). \tag{12}$$

Rewriting $a = T_0/T_\gamma$ and using the fact that $n_H a^3$ is given by ω_b (up to a factor predicted by nucleosynthesis), we find that $\dot{\tau}/T_0$ is a function of $T_\gamma, \varpi_b, \varpi_{cdm}$. Using $d/d\eta = aHT_\gamma d/dT_\gamma = T_0 H d/dT_\gamma$, we then find that Eq. (12) is satisfied for a temperature $T_\gamma = T_*$ independent of T_0, and depending only on ϖ_b, ϖ_{cdm}. For future reference, we write the corresponding fitting function that can be obtained by adjusting a numerical fit of Ref. [35],

$$T_* \approx 2970 \left(\frac{\varpi_m \text{ K}^3}{7.06 \times 10^{-3}}\right)^{0.0105} \left(\frac{\varpi_b \text{ K}^3}{1.1 \times 10^{-3}}\right)^{-0.028} \text{K}. \tag{13}$$

Thus, the *temperature of last-scattering T_* is independent of T_0* for some given ϖ_b, ϖ_{cdm}. Of course, the *redshift* of last-scattering z_* does depend on T_0 through $1 + z_* = T_*/T_0$, and so does the conformal time at last scattering $\eta_* \propto 1/T_0$.

The effective sound speed of the photon-baryon fluid $c_s = \frac{1}{\sqrt{3}}\left(1 + \frac{3}{4}\frac{\rho_b}{\rho_\gamma}\right)^{-1/2}$ is a function of T_γ, ϖ_b only. Therefore, the comoving sound horizon at last scattering r_s is such that $T_0 r_s$ is a function of ϖ_b, ϖ_{cdm} only:

$$r_s = \int_0^{\eta_*} c_s d\eta = \frac{1}{T_0} \int_{T_*}^\infty c_s(T_\gamma; \varpi_b) \frac{dT_\gamma}{H(T_\gamma; \varpi_m)}. \tag{14}$$

This implies that the *physical scale* of the sound horizon at recombination, $a_* r_s = (T_0/T_*)r_s$, is a function of ϖ_b, ϖ_{cdm} only, and does not depend on T_0.

The same argument holds true for the moment of baryon decoupling (also called the baryon drag time), which happens slightly after recombination. Therefore, the physical size of the sound horizon at baryon decoupling $r_{d, \text{phys}}$, which is important for the BAO measurements, does not depend on T_0. A useful fitting function for $r_{d, \text{phys}}$ can be obtained by combining Eq. (13) with the fit of Ref. [12],

$$r_{d, \text{phys}} = a_d r_d \approx 0.1386 \left(\frac{\varpi_m \text{ K}^3}{7.06 \times 10^{-3}}\right)^{-0.26}$$
$$\times \left(\frac{\varpi_b \text{ K}^3}{1.10 \times 10^{-3}}\right)^{-0.10} \text{Mpc}. \tag{15}$$

The CMB anisotropy power spectrum that we will discuss in 3.5 depends crucially on the physical photon diffusion damping scale at last scattering, which is of the form

$$a_* r_{\text{damp}} = 2\pi \left[\int_0^{\eta_*} \frac{\mathcal{D}(R)}{\dot{\tau}} d\eta\right]^{1/2}, \tag{16}$$

where $\mathcal{D}$ is a function of $R \equiv \frac{3\rho_b}{4\rho_\gamma}$ (see for instance [36]). Like for $a_* r_s$, some elementary steps show that this physical scale only depends on fundamental constants and on ϖ_b, ϖ_{cdm}.

3.4. Transfer functions and initial conditions

Transfer functions are solutions of the cosmological linear perturbation equations for each wavenumber k normalised in the super-Hubble regime, for instance, to $\mathcal{R}(k) = 1$. For fixed initial conditions, CMB anisotropy and large-scale structure observables depend on a number of such transfer functions evaluated at different epochs.

Another potential source of T_0-dependence is the normalization of transfer functions. The cosmological perturbations are characterized by the conformal comoving wavenumber k, which is equal to the physical wavenumber now (which is typically normalized as $a = 1$ now). Since the current Universe age depends on T_0, the comoving wavenumbers depend on it as well, as opposed to the *physical* wavenumbers. However, there is a way to rescale the conformal momenta such that the dynamics of cosmological perturbations do not depend on T_0.

It is a straightforward exercise to rewrite equations for linear cosmological perturbations in terms of T_γ rather than conformal time (starting from, e.g. [37]). By doing this, one can find that the transfer functions depend
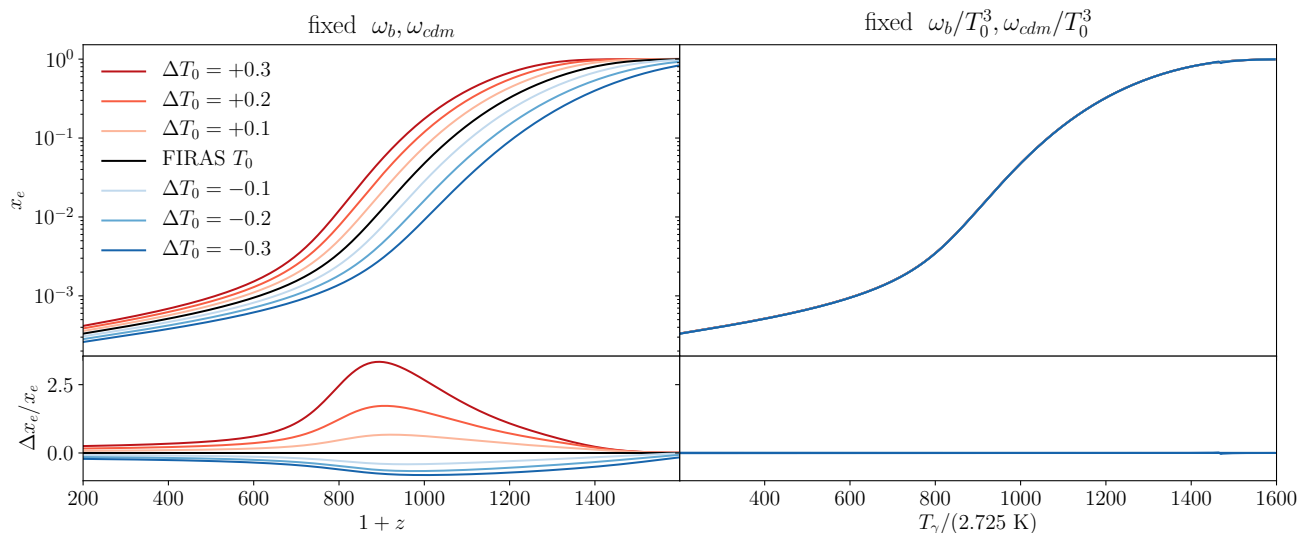
FIG. 1. Free-electron fraction x_e for different values of the present-day CMB monopole T_0. On the left panel, we keep ω_b, ω_{cdm} constant, and show x_e as a function of redshift, which leads to large variations when changing T_0, as found in Ref. [20]. On the right panel, we keep $\omega_b/T_0^3, \omega_{cdm}/T_0^3$ constant, and show x_e as a function of photon temperature. In terms of these rescaled variables, x_e is independent of T_0. In both cases, the Helium mass fraction Y_{He} is kept constant; this is consistent with BBN predictions only if ω_b/T_0^3 is kept constant.

on $T_\gamma, \varpi_b, \varpi_{cdm}, \Lambda$ and k/T_0, where k is the comoving wavenumber. This can be easily understood as follows. Instead of a set of comoving scales k that correspond to inverse physical scales at the current time, one can define another set of comoving scales $\tilde{k}$ coinciding with inverse physical scales *at a fixed photon temperature*. If we choose arbitrarily this temperature to be $T_\gamma = 1$, the two sets are related through $\tilde{k} = k/T_0$.

Then, two universes with the same $\varpi_b, \varpi_{cdm}, \Lambda$ have the same $\tilde{k}$-dependent transfer functions *at a given photon temperature*. Such universes are statistically identical if they further have the same $\tilde{k}$-dependent power spectrum $\Delta_{\mathcal{R}}^2$ of scalar fluctuations. In other words, the r.m.s. amplitudes of primordial fluctuations should be the same on the same physical scales in both universes. The simple power-law spectrum motivated by inflation is typically defined at some arbitrary pivot scale k_{P}, which should be appropriately rescaled in a Universe with different T_0. Alternatively, one could rescale the amplitude itself. Indeed, keeping k_{P} fixed, we may rewrite the primordial curvature power spectrum as a function of $\tilde{k} = k/T_0$ as follows:

$$\Delta_{\mathcal{R}}^2 = A_s(k/k_{\mathrm{P}})^{n_s-1} = A_s T_0^{n_s-1}(\tilde{k}/k_P)^{n_s-1}. \quad (17)$$

Thus, in the case of power-law initial conditions, our scaling scheme requires the combination $A_s T_0^{n_s-1}$ to be fixed.

We illustrate these points in Fig. 2, where we show the matter power spectrum for several values of T_0, but fixed ϖ_b, ϖ_c and $A_s T_0^{n_s-1}$, as a function of $\tilde{k} = k/T_0$. We see that it remains completely unaffected by T_0 when computed at the decoupling redshift z_{dec}, corresponding to the fixed energy scale T_*. However, when computing it *at the present time*, i.e. at an energy scale T_0, its amplitude clearly varies with T_0, as expected.

The value of the cosmological constant used to produce these plots is extracted from θ_s, which is fixed to the Planck best-fit value. This way, varying T_0 changes the amount of time elapsed since recombination until today, which changes the relative current fraction of the cosmological constant energy density w.r.t matter density. This leads to a different growth history and hence affects the amplitude of the power spectrum at $z = 0$. These effects will be discussed in detail momentarily.

3.5. Primary CMB anisotropies

There are two different contributions to the CMB primary (unlensed) power spectra. On small scales, anisotropies are mostly sourced by photon, baryon and metric fluctuations at last scattering, whose transfer functions contain damped oscillatory features associated
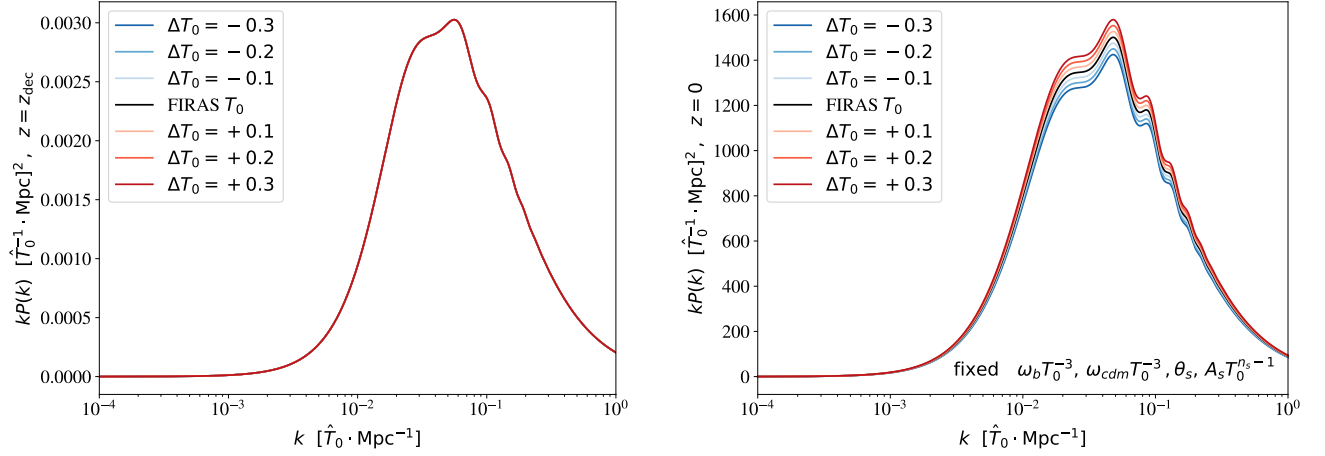
FIG. 2. Effect of a variation of T_0 (quoted in Kelvins) on the matter power spectrum at the time of last scattering (left panel) and today (right panel). The combinations $\omega_b/T_0^3, \omega_{cdm}/T_0^3, \theta_s$ and $A_s T_0^{n_s-1}$ are kept constant. In this case, the matter power spectrum computed at the time of last scattering (left panel) is independent of T_0. A constant θ_s fixes the ratio between T_0 and Λ. This choice does not noticeably affect the physics at recombination, but introduces a correlation between T_0 and the growth factor seen when we evaluate the power spectrum at the present time (right panel). We use the units $\hat{T}_0 \cdot \text{Mpc}^{-1}$ ($\hat{T}_0 \equiv T_0/T_{0,\,\text{FIRAS}}$), such that all spectra are shown as functions of the same rescaled wavevector $\tilde{k} = k/T_0$.

to the physical sound horizon scale $a_* r_s$ and damping scale $a_* r_{\text{damp}}$. On large scales, the temperature spectrum receives an additional contribution from the late-time integrated Sachs-Wolfe (ISW) effect (see e.g. [38]), resulting from the time variation of gravitational potentials when the cosmological constant becomes important.

We have seen that for fixed ϖ_b, ϖ_{cdm}, Λ and $A_s T_0^{n_s-1}$, not only the background evolution $H(T_\gamma)$ is independent of T_0, but so are the temperature of last scattering T_*, the transfer functions expressed in terms of $(T_\gamma, \tilde{k})$, and all r.m.s. fluctuations as a function of the same two variables. Nevertheless, the unlensed CMB spectra still depend on T_0, for the two following reasons:

1. The CMB spectra are inferred from spherical maps, and thus expanded in multipoles rather than wavenumbers. The (Legendre) transformation from wavenumber to multipole space involves implicitly the angular diameter distance D_A, which contains an integral over the expansion history relative to the current time, and thus depends on T_0, as anticipated in 3.2. For instance, the angular diameter distance to the last scattering surface reads

$$D_A(T_*) = a_* \int_{T_0}^{T_*} \frac{dT_\gamma}{T_0 H(T_\gamma)} = \frac{1}{T_*} \int_{T_0}^{T_*} \frac{dT_\gamma}{H(T_\gamma)}, \quad (18)$$

and depends explicitly on T_0 through the lower integration boundary. This means that the scaling that we discussed so far preserves the exact shape of the CMB unlensed spectra C_ℓ, on all scales for the polarization spectrum, and on small scales that are unaffected by the late ISW effect for the temperature spectrum. However it shifts these spectra horizontally to larger or smaller multipoles depending on the value of T_0.

2. The late ISW effect depends essentially on the amount of expansion during Λ domination, given by $1 + z_\Lambda = T_\gamma^\Lambda/T_0$. For a fixed Λ, the photon temperature at matter-to-Λ equality T_γ^Λ is fixed, but z_Λ depends explicitly on T_0. Thus late ISW contribution to the large scale temperature spectrum depends on T_0.

We show the variations of CMB power spectra in Fig. 3 with different T_0. On the left column, we keep $\omega_b, \omega_{cdm}, H_0$ and A_s constant, recovering the results of Refs. [20, 21]. On the right, we keep $\omega_b/T_0^3, \omega_{cdm}/T_0^3$ and $A_s T_0^{n_s-1}$ constant; we moreover keep the angular scale $\theta_s \equiv a_* r_s/D_A(T_*)$ fixed. The CLASS code [39] automatically adjusts Λ – or equivalently, $H_0 \simeq \left[\frac{\Lambda}{3} + \gamma_{100}^2 \varpi_m T_0^3\right]^{1/2}$ – to produce any requested input θ_s.

We see that when these parameters are kept fixed, the TT, TE, and EE CMB spectra computed by the CLASS code [39] are exactly invariant on small scales when T_0 varies. However, this transformation preserves neither $(\Lambda, T_\gamma^\Lambda)$ and the absolute energy scale of Λ domination, nor $(\Omega_\Lambda, z_\Lambda)$ and the amount of expansion during Λ domination. Thus the amplitude of the late ISW effect is different, which can be seen as residual variations on large angular scales in Fig. 3. These large scales are dominated by cosmic variance and are thus poorly constrained by observations. As a consequence, CMB observations alone would only poorly constrain T_0 due to the large geometric degeneracy between T_0 and H_0.

We can understand the direction of the $T_0 - H_0$ degeneracy analytically as follows. The integral in eq. (18) is dominated by the low-temperature end, for which we may neglect the radiation contribution to $H(T_\gamma)$, i.e.

$$H(T_\gamma) \approx \gamma_{100}\sqrt{h^2 + \varpi_m(T_\gamma^3 - T_0^3)}. \qquad (19)$$

Since $T_* \gg T_0$, we may further take the upper boundary to infinity, and arrive at

$$\gamma_{100}D_A(T_*) \approx \frac{1}{T_*}\int_{T_0}^{\infty}\frac{dT}{\sqrt{h^2 + \varpi_m(T^3 - T_0^3)}}$$
$$= \frac{T_0}{hT_*}\int_1^{\infty}\frac{dx}{\sqrt{1 + \Omega_m(x^3 - 1)}} \equiv \frac{T_0}{hT_*}\mathcal{I}(\Omega_m), \quad (20)$$

where $\Omega_m \equiv \varpi_m T_0^3/h^2 = \omega_m/h^2$ is the usual matter density fraction, and the function $\mathcal{I}(\Omega_m)$ can be written in terms of a hypergeometric function.

Assuming the Planck+FIRAS best-fit values for ϖ_m, T_0 and h for numerical calculations, we obtain,

$$\left.\frac{\partial \ln D_A}{\partial \ln T_0}\right|_{\text{Planck}} \approx -0.22\,, \quad \left.\frac{\partial \ln D_A}{\partial \ln h}\right|_{\text{Planck}} \approx -0.19\,, \qquad (21)$$

at constant ϖ_m. Thus, around the Planck best-fit cosmology, the angular diameter distance is mostly a function of the combination $H_0 T_0^{1.2}$, and we expect an approximate degeneracy $H_0 \propto T_0^{-1.2}$ at fixed ϖ_b, ϖ_{cdm}. This estimates agrees with the degeneracy found in our MCMC analysis, see Fig. 5. The details of this analysis will be discussed in the next Section.

3.6. CMB lensing

We have already seen that keeping ω_b/T_0^3, ω_m/T_0^3 and θ_s constant does not preserve the amount of expansion taking place between last scattering and matter-to-Λ equality, given by T_*/T_γ^Λ, nor during Λ domination, given by T_γ^Λ/T_0 (where T_γ^Λ depends on T_0). A different ratio T_γ^Λ/T_0 implies a different amplitude of the late ISW contribution to large-scale temperature anisotropies. The variation of T_0 should be further imprinted through the CMB lensing effect, which also correlates with the late-time decay factor of metric fluctuations during Λ domination. Besides, the CMB lensing spectrum should be shifted horizontally by a different angular diameter distance to small redshifts. As is usually the case when changing the redshift of matter-to-Λ equality, these different effects nearly compensate each other at the level of the lensing potential on small angular scales, and appear mainly at $\ell \lesssim 100$ [40]. This is confirmed in Fig. 4, where we show the power spectrum of deflection angle for different values of T_0.

The smoothing of acoustic peaks in the CMB temperature and polarization spectra is sensitive to a broad range of multipoles around the peak of the deflection-angle power spectrum C_l^{dd} shown in Fig. 4. Thus, this smoothing is slightly impacted by a change of T_0 when $\omega_b/T_0^3, \omega_{cdm}/T_0^3, \theta_s$ and $A_s T_0^{n_s-1}$ are kept constant. Together with the late ISW effect, this is one of the two mechanisms through which the (lensed) CMB spectra are sensitive to T_0. Finally, CMB lensing extraction allows to measure the deflection spectrum and can marginally increase the sensitivity of CMB experiments to T_0, although this technique has more sensitivity to scales $\ell \geq 70$ at which the effect of the CMB temperature on C_l^{dd} is gradually suppressed.

In conclusion, we see that the geometric degeneracy of T_0 and H_0 in CMB anisotropies is broken by the ISW effect on large scales, as well as gravitational lensing. We find that the two have comparable constraining power, with the ISW effect being dominant, and lensing reducing error bars on T_0 and H_0 by an additional $\sim 30\%$.

3.7. Large-scale structure

Let us discuss now the impact of varying T_0 on large-scale structure. For simplicity, let us focus on the baryon acoustic oscillation (BAO) measurements, which are widely used to break the geometric degeneracy of CMB data.
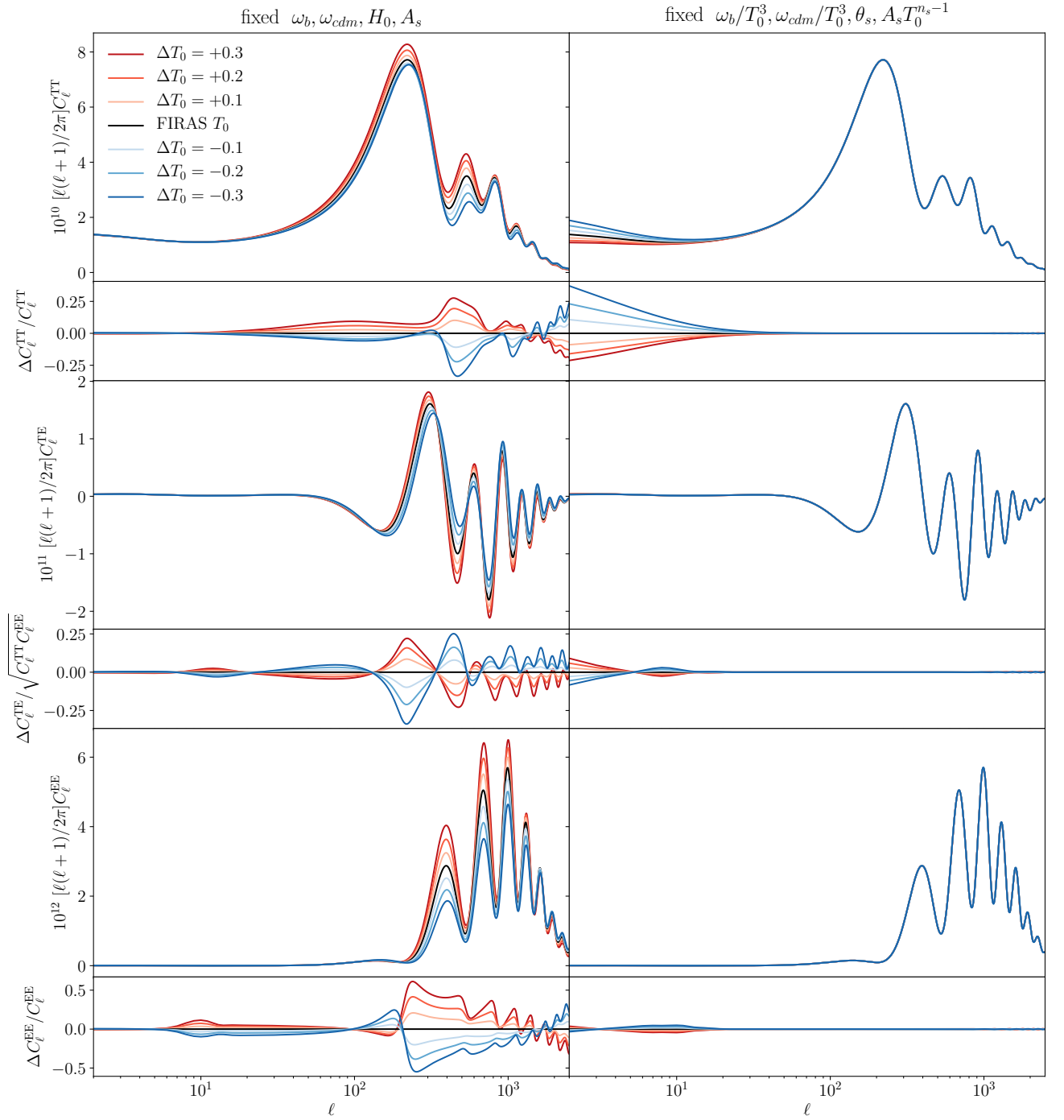
The galaxy distribution mapped by spectroscopic sur-

FIG. 3. Effect of a variation of T_0 (quoted in Kelvins) on the lensed TT, TE and EE CMB power spectra. In the left column, $\omega_b, \omega_{cdm}, H_0$ and A_s are kept constant, as in Refs. [20, 21]. In the right column, the combinations $\omega_b/T_0^3, \omega_{cdm}/T_0^3, \theta_s$ and $A_s T_0^{n_s-1}$ are kept constant. With the latter choice of constant parameters, CMB power spectra are independent of T_0 on small scales, but do depend on T_0 at large scales through the ISW effect. In both cases, $\tau_{\rm reio}$ is kept constant.

veys is a three-dimensional observable, which is characterized by angles and redshifts. This can be contrasted with the CMB, whose BAO pattern is only observed in projection onto the two-dimensional last-scattering sphere.
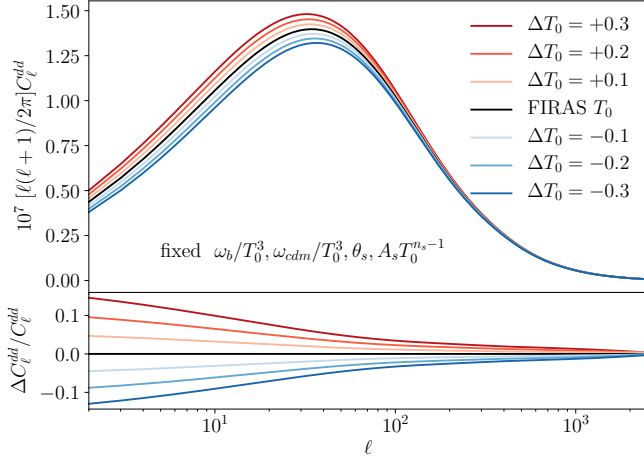
The galactic BAO is usually probed through the

FIG. 4. Power spectrum of the lensing deflection angle as a function of T_0, for fixed $\omega_b/T_0^3, \omega_c/T_0^3, \theta_s$ and $A_s T_0^{n_s-1}$. Note that this power spectrum is computed entirely within the Limber approximation for simplicity.

position-space two-point correlation function, which peaks at the spatial separation corresponding to the physical size of the BAO scale at the observed epoch. This scale is not directly observed, because a galaxy survey only measures the angular position of the galaxies and their redshift. To convert these coordinates into a grid of comoving distances one typically assumes some fiducial cosmology. As long as the difference between the distances in fiducial and true cosmologies are small, the geodesic distance between a pair of galaxies can be described by the so-called Alcock-Paczynski (AP) scaling parameters[6],

$$\alpha_\parallel = \frac{H_{\text{fid}}(z)}{H(z)}, \quad \alpha_\perp = \frac{D_A(z)}{D_{A,\text{fid}}(z)}. \tag{22}$$

$\alpha_\parallel$ and $\alpha_\perp$ capture, correspondingly, the radial and angular fractions of the separation between two galaxies. The description in terms of the AP parameters is adequate for space-times with small spatial curvature gradients that behave globally like the Friedman-Robertson-Walker-Lemaitre Universe [44–46]. Thus, it will be sufficient for our analysis within the flat ΛCDM model.

The isotropic component of the galaxy distribution is mostly sensitive to the following combination of the AP parameters:

$$\alpha = (\alpha_\parallel \alpha_\perp^2)^{1/3}, \tag{23}$$

which describes how a small spatial volume "reconstructed" from the observed volume of angles and redshifts rescales due to a difference between the true and fiducial cosmologies.

It is customary to parametrize the galactic BAO with an effective angular size of the acoustic peak in the two-point correlation function [38],

$$\theta_{\text{BAO}} = \frac{r_d}{D_V(z_{\text{eff}})}, \tag{24}$$

where z_{eff} is the effective (weighted) redshift (see e.g. Eq. (9) from Ref. [47]) and D_V is the effective comoving volume-averaged distance to the galaxy sample [44],

$$D_V(z_{\text{eff}}) = ((1 + z_{\text{eff}})^2 D_A^2(z_{\text{eff}}) z_{\text{eff}}/H(z_{\text{eff}}))^{1/3}. \tag{25}$$

Physically, θ_{BAO} can be thought of as a scale of the BAO in the angular two-point galaxy correlation function, which is averaged over the redshift bin of a survey. It is a very close counterpart of θ_s measured in the CMB data. We stress that the AP conversion is only a technical tool to extract this angle from the data.[7]

The anisotropic part of the galaxy BAO signal is characterized by another combination of the AP parameters,

$$\epsilon = \left(\frac{\alpha_\parallel}{\alpha_\perp}\right)^{1/3} - 1, \tag{26}$$

which describes how the difference between the true and fiducial cosmology affects the relative scaling between the radial and transverse distances. The combination of isotropic and anisotropic BAO signals allows one to separately constrain the parameters

$$\theta_{\text{BAO},\parallel} \equiv r_d H(z_{\text{eff}}) \quad \text{and} \quad \theta_{\text{BAO},\perp} \equiv \frac{r_d}{(1 + z_{\text{eff}})D_A(z_{\text{eff}})}. \tag{27}$$

Note that the anisotropic BAO signal is a quite weak probe of cosmological parameters in minimal models

---

[6] See the original paper [41] and Refs. [42, 43] for the first applications of the scaling parameters in the form used nowadays, e.g. in the official BOSS data analysis [30].

---

[7] Mathematically, it is equivalent to extracting the BAO scale from the angular power spectrum of the observed galaxies, as it is done for the CMB. An advantage of the distance conversion approach is that it allows one to directly compare the data to a 3d power spectrum model without having to project it onto the sky. A discussion on this point can be found, e.g. in Ref. [48].
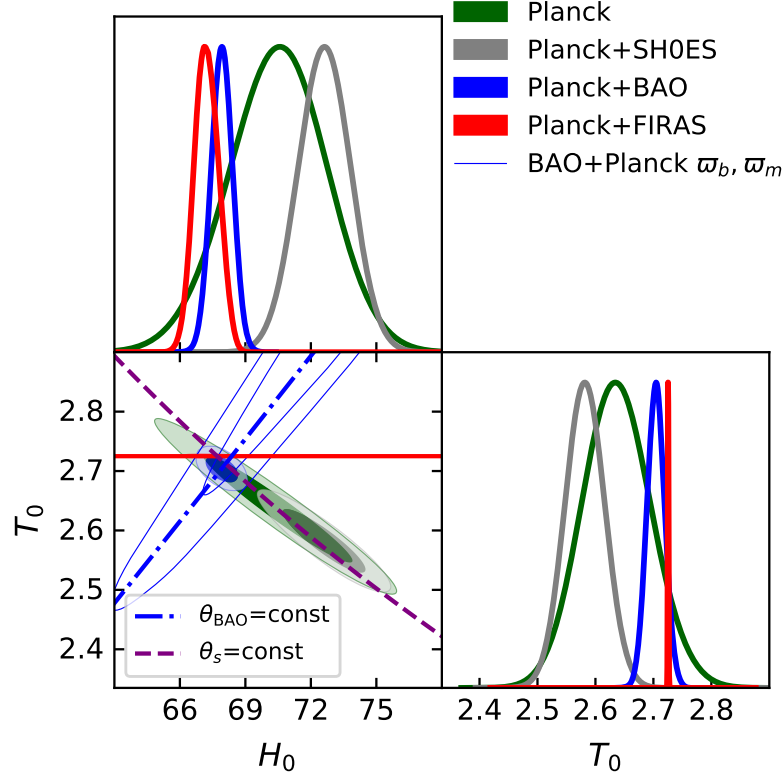
FIG. 5. Posterior distribution for T_0 and H_0 extracted from the analysis of the following datasets: Planck 2018 data, Planck plus the SH0ES H_0 prior, Planck plus the BOSS DR12 BAO, Planck plus the FIRAS T_0 prior, and finally the BAO plus the Planck priors on ϖ_b, ϖ_m. We stress that T_0 was varied in all these analyses. A horizontal solid red line marking the FIRAS value is put for illustrative purposes. The purple dotted-dashed line shows the degeneracy direction $H_0 \propto T_0^{-1.2}$ that roughly produces a fixed CMB acoustic angle θ_s, whereas the blue long dashed line shows the degeneracy $H_0 \propto T_0^{0.86}$ expected to produce a fixed BAO acoustic angle θ_{BAO} (see the main text for more details).

[8, 41, 43]. The base ΛCDM model with varied CMB temperature T_0 considered in this paper also belongs to this class.

Importantly, the effective redshift of a galaxy sample z_{eff} is always known because it is measured directly from the data. This should be contrasted with the CMB observations. If the physical sound horizon at decoupling $r_{d,\,\mathrm{phys}}$ is fixed, its comoving size depends on the unknown decoupling redshift z_{dec} and hence T_0,

$$r_d = r_{d,\,\mathrm{phys}}\Big|_{z_{\mathrm{dec}}} (1 + z_{\mathrm{dec}}). \qquad (28)$$

The effective volume-averaged distance to the galaxies has a different dependence on cosmological parameters compared to $D_A(z_*)$. Indeed, performing a calculation

similar to Eq. (21) we find[8]

$$\frac{\partial \ln D_V}{\partial \ln H_0}\bigg|_{z_{\mathrm{eff}}=0.38} = -0.78\,, \quad \frac{\partial \ln D_V}{\partial \ln T_0}\bigg|_{z_{\mathrm{eff}}=0.38} = -0.33\,. \qquad (29)$$

Combining it with Eq. (28) we obtain

$$\frac{\partial \ln \theta_{\mathrm{BAO}}}{\partial \ln H_0}\bigg|_{z_{\mathrm{eff}}=0.38} = 0.78\,, \quad \frac{\partial \ln \theta_{\mathrm{BAO}}}{\partial \ln T_0}\bigg|_{z_{\mathrm{eff}}=0.38} = -0.67\,. \qquad (30)$$

Thus, the BAO angle θ_{BAO} constrains the combination $H_0 T_0^{-0.86}$, which is quite orthogonal to the line of constant $H_0 T_0^{1.2}$ probed by the CMB. This allows one to break the degeneracy between T_0 and H_0 when the galaxy BAO is combined with Planck.

————

[8] Here we use $z_{\mathrm{eff}} = 0.38$, the effective redshift of the low-z BOSS galaxy sample [30].

This effect is illustrated in Fig. 5, where we show the $H_0 - T_0$ posterior extracted from the BOSS DR12 BAO data [34]. To obtain this posterior, we have fitted the BAO data with *minimal priors* from Planck 2018 data, namely the baryon- and matter-to-photon ratios ϖ_b, ϖ_m. The use of these priors is motivated by the following argument. When we eventually combine BAO and Planck 2018, the ϖ_b, ϖ_m limits will be totally dominated by Planck, because they are measured to 1% precision from the shape of the CMB spectra independently of the late-time geometric expansion.

In passing, it is worth noting that the anisotropic BAO signal, in principle, allows one to separately measure T_0 and H_0 from the BAO data alone if the priors on ϖ_b, ϖ_m are imposed. Indeed, the full BAO signal is summarized in terms of two parameters, $r_d/D_A(z)$ and $r_d H(z)$, which depend on ϖ_b, ϖ_m, H_0 and T_0 in our model (see Eq. (19) and Eq. (28)). Once ϖ_b, ϖ_m are fixed by the priors, we are left with two parameters to constrain H_0 and T_0, which allows one to eventually break the degeneracy between them. This explains why the $H_0 - T_0$ posterior contour from the BAO in Fig. 5 is not an infinite line. However, as we can see from this plot, even though the T_0 and H_0 measurements from the BAO alone are possible in principle, the resulting constraints are quite loose because the anisotropic part of the BAO signal is a very weak function of cosmological parameters. In combination with Planck only the best measured isotropic BAO part matters.

Additionally, one can constrain the peculiar velocity fluctuation r.m.s. $f\sigma_8$ from redshift-space distortions. All these pieces of information break the geometric degeneracies between the late-time parameters $\omega_{cdm}, \omega_b, h$ and T_0.

Alternatively, one can break the geometric degeneracy and measure T_0 from the Planck data by the local measurement from SH0ES that yields a direct prior on H_0. In this paper we will focus on these two possibilities: the BAO from galaxy surveys and local measurement of H_0 by Cepheid-calibrated supernovae.

4. RESULTS

We will now fit our $T_0 - \Lambda$CDM model to cosmological data, with a flat prior on the seven parameters motivated by the previous discussion: the CMB temperature itself, T_0, plus the six combinations that determine the CMB spectra independently of T_0, up to the late ISW and CMB lensing effects: $\{\omega_b \hat{T}_0^{-3}, \omega_{cdm} \hat{T}_0^{-3}, \theta_s, \ln(10^{10} A_s \hat{T}_0^{1+n_s}), \tau_{\rm reio}, n_s\}$, with $\hat{T}_0 = T_0/T_{0,\,\rm FIRAS}$.

Note that in section 3.4, we argued that the quantity fixing the overall normalization of the CMB spectra independently of T_0 was $A_s T_0^{n_s-1}$. This was correct at the level of the dimensionless spectra C_l that would be derived from relative fluctuation maps $\Delta T/T_0, Q/T_0, U/T_0$ (where Q, U are the Stokes parameters). However, being calibrated to the CMB dipole, Planck measures primarily the spectra of the absolute fluctuations maps $\Delta T, Q, U$ expressed in Kelvins. The combination that fixes the global amplitude of the observed spectra independently of T_0 is thus $A_s T_0^{n_s-1} \times T_0^2$. This explains why we take $\ln(10^{10} A_s \hat{T}_0^{1+n_s})$ as one of our basis parameters (choosing instead $\ln(10^{10} A_s \hat{T}^{n_s-1})$ would lead to a strong degeneracy with T_0).

The triangle plots with posterior densities and marginalized distributions for the parameters of our $T_0 - \Lambda$CDM model (including the derived parameter H_0) are shown in Fig. 6. For comparison, we also display the contours obtained with a baseline Planck analysis with T_0 fixed to the FIRAS prior. The results of this analysis are in good agreement with the ones reported by the Planck collaboration [4].[9] The marginalized limits are presented in Table I.

We can clearly see that releasing T_0 in the fit makes the Planck data compatible with the SH0ES H_0 measurements. As anticipated, we observe that the posterior distribution of the parameters $\{\omega_b \hat{T}_0^{-3}, \omega_{cdm} \hat{T}_0^{-3}, \ln(10^{10} A_s \hat{T}_0^{1+n_s}), \theta_s\}$ are almost the same in the fit with free T_0 and with T_0 fixed to the FIRAS value. There are some small shifts (well below statistical uncertainties) which are most likely produced by residual correlations between primary and secondary effects (e.g. the CMB lensing affects the height of the acoustic peaks).

Overall, the observed shifts are consistent with the typical effect of adding one parameter to the fit. The effective $\chi^2_{\rm eff}$ of Planck reduces only by $\Delta\chi^2_{\rm eff} = -1.7$ when

———

[9] We have found some small shifts in the cosmological parameters, which resulted from using `HyRec` instead of `recfast` [23, 49]. These shifts are very small relative to statistical uncertainties.
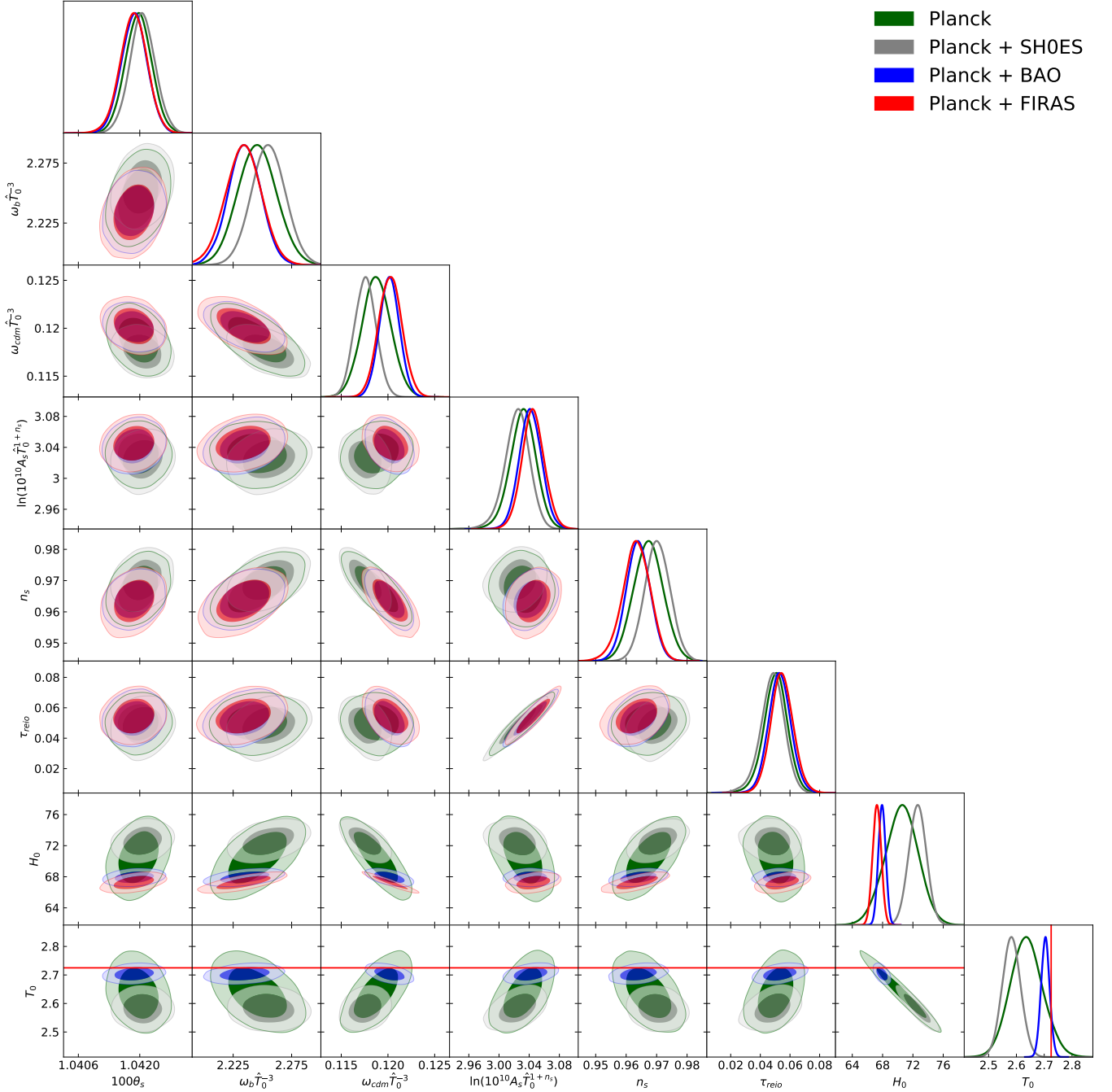
FIG. 6. Posterior distributions and marginalized 68% and 95% confidence contours for the cosmological parameters of the $T_0 - \Lambda\text{CDM}$ model fitted to Planck (in green), Planck+SH0ES (in gray), and Planck + BAO (in blue). For comparison, we also show the result of the Planck baseline analysis with T_0 fixed to the FIRAS best-fit value 2.7255 K (in red).

T_0 is allowed to vary.

The geometric degeneracy between H_0 and T_0 gets broken once we impose the H_0 prior from SH0ES. In this case the fit to CMB data degrades noticeably. Indeed the effective χ^2_{eff} of the Planck likelihoods computed at

the best-fitting point to the Planck+SH0ES dataset is worse than that computed at the best-fitting point to Planck+FIRAS by:

$$\Delta\chi^2_{\text{eff}} \equiv \chi^2_{\text{eff}}(\text{Planck+SH0ES}) - \chi^2_{\text{eff}}(\text{Planck+FIRAS})$$
$$= 2793.14 - 2775.64 = 17.5\,. \tag{31}$$

Parameter \ Dataset	Planck + FIRAS	Planck	Planck + SH0ES	Planck + BAO
$100\,\omega_b\hat{T}_0^{-3}$	$2.235^{+0.015}_{-0.014}$	$2.245^{+0.016}_{-0.016}$	$2.255^{+0.015}_{-0.015}$	$2.235^{+0.015}_{-0.014}$
$\omega_{cdm}\hat{T}_0^{-3}$	$0.1202^{+0.0012}_{-0.0012}$	$0.1188^{+0.0015}_{-0.0015}$	$0.1176^{+0.0011}_{-0.0011}$	$0.1202^{+0.0011}_{-0.0011}$
$100\,\theta_s$	$1.0419^{+0.00029}_{-0.0003}$	$1.042^{+0.0003}_{-0.0003}$	$1.04206^{+0.00029}_{-0.00029}$	$1.042^{+0.00029}_{-0.00029}$
$\tau_{\rm reio}$	$0.05468^{+0.0069}_{-0.0078}$	$0.05014^{+0.0085}_{-0.0077}$	$0.04791^{+0.0085}_{-0.0085}$	$0.0531^{+0.0075}_{-0.0077}$
$\ln(10^{10}A_s\hat{T}_0^{1+n_s})$	$3.045^{+0.014}_{-0.015}$	$3.029^{+0.018}_{-0.016}$	$3.021^{+0.017}_{-0.017}$	$3.041^{+0.014}_{-0.015}$
n_s	$0.9637^{+0.0041}_{-0.0043}$	$0.9673^{+0.0049}_{-0.005}$	$0.9783^{+0.0042}_{-0.0042}$	$0.964^{+0.0039}_{-0.004}$
T_0	$2.72548^{+0.00057}_{-0.00057}$	$2.636^{+0.057}_{-0.061}$	$2.582^{+0.033}_{-0.033}$	$2.704^{+0.015}_{-0.016}$
$100\,\omega_b$	$2.235^{+0.015}_{-0.014}$	$2.035^{+0.12}_{-0.14}$	$1.918^{+0.074}_{-0.074}$	$2.183^{+0.042}_{-0.044}$
ω_{cdm}	$0.1202^{+0.0012}_{-0.0012}$	$0.1077^{+0.0075}_{-0.0089}$	$0.1^{+0.0042}_{-0.0042}$	$0.1174^{+0.0019}_{-0.0017}$
Ω_Λ	$0.6834^{+0.0075}_{-0.0075}$	$0.7392^{+0.041}_{-0.029}$	$0.7724^{+0.016}_{-0.016}$	$0.6968^{+0.0085}_{-0.0083}$
H_0	$67.28^{+0.53}_{-0.55}$	$70.5^{+2.3}_{-2.1}$	$72.6^{+1.2}_{-1.2}$	$67.92^{+0.49}_{-0.49}$
σ_8	$0.8117^{+0.0057}_{-0.006}$	$0.8348^{+0.017}_{-0.015}$	$0.8956^{+0.01}_{-0.01}$	$0.8182^{+0.008}_{-0.0079}$

TABLE I. Mean values and 68% CL minimum credible intervals for the parameters of the $T_0 - \Lambda$CDM model fitted to Planck+FIRAS, Planck only, Planck + SH0ES, and Planck + BAO. For comparison, we also quote in the leftmost column the results obtained for the baseline Planck analysis with T_0 fixed to the FIRAS value in the leftmost column. We assumed flat priors on the first seven parameters, which are defined in the text. The last five rows show derived parameters. H_0 is quoted in km/s/Mpc, T_0 is quoted in units of Kelvin, and $\hat{T}_0 \equiv T_0/T_{0,\,\rm FIRAS}$.

In the Planck+SH0ES analysis, the best-fit T_0 is significantly smaller than the FIRAS value. This was to be expected from the CMB geometric degeneracy $H_0 \propto T_0^{-1.2}$, which requires a smaller T_0 in order to be consistent with the larger H_0 prior from SH0ES, given the very well constrained angle θ_s. The optimal values of T_0 from Planck + SH0ES and FIRAS are separated by $\Delta T_0 = 0.14$ K, which corresponds to 4.2 Planck + SH0ES standard deviations. Importantly, the Hubble tension gets fully translated into the 4.2σ-tension between FIRAS and Planck+SH0ES.

If we use the BAO to break the geometric degeneracy instead of SH0ES, we obtain a measurement of T_0 that agrees with the FIRAS measurement within 95% CL. The small residual difference between the two measurements (1.4σ) is compatible with a statistical fluctuation. The goodness of fit to Planck data does not degrade much in this case,

$$\Delta\chi^2_{\rm eff} \equiv \chi^2_{\rm eff}(\text{Planck+BAO}) - \chi^2_{\rm eff}(\text{Planck+FIRAS})$$
$$= 2777.02 - 2775.64 = 1.38\,. \tag{32}$$

Overall, we observe good agreement between Planck+BAO and FIRAS.

In this work, for concision, we did not discuss the constraints coming from the measurement of the amplitude of the matter power spectrum near the present time. We can briefly mention that weak lensing surveys often report an estimate of the parameter combination $S_8 \equiv \sigma_8(\Omega_m/0.3)^{0.5}$, and that the degeneracy discussed in this work is such that smaller values of T_0 lead to smaller values of S_8. For instance, our $T_0 - \Lambda$CDM best-fit model to Planck+SH0ES has $S_8 \simeq 0.78$, in very good agreement with KIDs and DES measurements [50–52]. Thus this model would not be disfavored on the basis of weak lensing data only – but as we explained, it is disfavoured instead by BAO and FIRAS data.

5. CONCLUSIONS

In this paper, we have given a detailed description of the effects of the CMB temperature monopole T_0 on cosmological observables, namely CMB anisotropies and large-scale structure. We have shown that cosmological background quantities and perturbations are independent of T_0 when computed at fixed baryon-to-photon

and dark matter-to-photon *number ratios*, and at fixed energy scales. The *observed* CMB anisotropy still depend on T_0, however, as this parameter quantifies the energy scale at the present time, from which observations are carried. The most significant effect of T_0 on CMB anisotropies is to change the angular diameter distance to the surface of last scattering, which is degenerate with a change of the Hubble parameter H_0. This geometric degeneracy approximately translates to the parameter degeneracy $H_0 \propto T_0^{-1.2}$.

The standard procedure to break the CMB-anisotropy geometric degeneracy is to include the very tight T_0 measurement from FIRAS. This leads to a measurement of the Hubble parameter H_0, with the well-known tension with the SH0ES measurement. In this work, we considered whether removing the FIRAS prior on T_0 and breaking the geometric degeneracy by different means might help alleviate the Hubble tension.

First, we showed, for the first time, that CMB anisotropy data *alone* can be used to measure T_0 and H_0 simultaneously. Indeed, the geometric degeneracy is not exact: it is broken on large angular scales by the integrated Sachs-Wolfe effect, as well as by gravitational lensing. From Planck data alone, we extract the 2% measurement $T_0 = 2.636^{+0.057}_{-0.061}$ K. While this results in a much looser bound on $H_0 = 70.5^{+2.3}_{-2.1}$ km/s/Mpc, other fundamental cosmological parameters (such as the baryon-to-photon number ratio) are mostly unaffected.

Second, rather than breaking the geometric degeneracy by including the FIRAS prior on T_0, thus inferring H_0, we use the SH0ES prior on H_0, and thus, for the first time, obtain an *independent measurement* of T_0 from Planck and SH0ES, $T_0 = 2.582 \pm 0.033$ K. This measurement is in strong (4.2σ) tension with the FIRAS measurement. Thus the H_0 tension between (Planck + FIRAS) and SH0ES can be fully recast as a T_0 tension between (Planck + SH0ES) and FIRAS. This simple result should serve as a reminder that the fundamental culprits of tensions are not necessarily any single parameter whose measurements differ between different dataset.

One may also break the $T_0 - H_0$ geometric degeneracy by including BAO data, as was done in past analyses. In that case, one finds that the resulting T_0 is consistent with that measured by FIRAS, and the measured H_0 is in tension with SH0ES. The BAO measurement thus seems to arbiter in favor of Planck + FIRAS, and disfavor SH0ES. Still, the Hubble tension – perhaps better named the Hubble-Penzias-Wilson tension – remains to be definitively solved.

---

[1] A. G. Riess, S. Casertano, W. Yuan, L. M. Macri, and D. Scolnic, Astrophys. J. **876**, 85 (2019), arXiv:1903.07603 [astro-ph.CO].

[2] M. J. Reid, D. W. Pesce, and A. G. Riess, Astrophys. J. **886**, L27 (2019), arXiv:1908.05625 [astro-ph.GA].

[3] K. C. Wong *et al.*, (2019), arXiv:1907.04869 [astro-ph.CO].

[4] N. Aghanim *et al.* (Planck), (2018), arXiv:1807.06209 [astro-ph.CO].

[5] T. M. C. Abbott *et al.* (DES), Mon. Not. Roy. Astron. Soc. **480**, 3879 (2018), arXiv:1711.00403 [astro-ph.CO].

[6] A. Cuceu, J. Farr, P. Lemos, and A. Font-Ribera, (2019), arXiv:1906.11628 [astro-ph.CO].

[7] N. Schöneberg, J. Lesgourgues, and D. C. Hooper, (2019), arXiv:1907.11594 [astro-ph.CO].

[8] M. M. Ivanov, M. Simonovic, and M. Zaldarriaga, (2019), arXiv:1909.05277 [astro-ph.CO].

[9] G. D'Amico, J. Gleyzes, N. Kokron, D. Markovic, L. Senatore, P. Zhang, F. Beutler, and H. Gil-Marín, (2019),

---

arXiv:1909.05271 [astro-ph.CO].

[10] T. Colas, G. D'amico, L. Senatore, P. Zhang, and F. Beutler, (2019), arXiv:1909.07951 [astro-ph.CO].

[11] O. H. Philcox, M. M. Ivanov, M. Simonović, and M. Zaldarriaga, arXiv:2002.04035 [astro-ph.CO].

[12] E. Aubourg et al., Phys. Rev. **D92**, 123516 (2015), arXiv:1411.1074 [astro-ph.CO].

[13] P. Lemos, E. Lee, G. Efstathiou, and S. Gratton, Mon. Not. Roy. Astron. Soc. **483**, 4803 (2019), arXiv:1806.06781 [astro-ph.CO].

[14] M. Rigault et al., Astrophys. J. **802**, 20 (2015), arXiv:1412.6501 [astro-ph.CO].

[15] C. S. Kochanek, (2019), arXiv:1911.05083 [astro-ph.CO].

[16] K. Blum, E. Castorina, and M. Simonović, (2020), arXiv:2001.07182 [astro-ph.CO].

[17] L. Knox and M. Millea, (2019), arXiv:1908.03663 [astro-ph.CO].

[18] D. J. Fixsen, E. S. Cheng, J. M. Gales, J. C. Mather, R. A. Shafer, and E. L. Wright, Astrophys. J. **473**, 576 (1996), arXiv:astro-ph/9605054 [astro-ph].

[19] D. J. Fixsen, Astrophys. J. **707**, 916 (2009), arXiv:0911.1955 [astro-ph.CO].

[20] J. Chluba and R. A. Sunyaev, Astron. Astrophys. (2007), 10.1051/0004-6361:20078200, [Astron. Astrophys.478,L27(2008)], arXiv:0707.0188 [astro-ph].

[21] J. Hamann and Y. Y. Y. Wong, JCAP **0803**, 025 (2008), arXiv:0709.4423 [astro-ph].

[22] J. Yoo, E. Mitsou, Y. Dirian, and R. Durrer, Phys. Rev. **D100**, 063510 (2019), arXiv:1905.09288 [astro-ph.CO].

[23] P. A. R. Ade et al. (Planck), Astron. Astrophys. **594**, A13 (2016), arXiv:1502.01589 [astro-ph.CO].

[24] E. Di Valentino et al. (CORE), JCAP **1804**, 017 (2018), arXiv:1612.00021 [astro-ph.CO].

[25] T. Brinckmann and J. Lesgourgues, (2018), arXiv:1804.07261 [astro-ph.CO].

[26] N. Aghanim et al. (Planck), (2019), arXiv:1907.12875 [astro-ph.CO].

[27] S. Seager, D. D. Sasselov, and D. Scott, Astrophys. J. **523**, L1 (1999), arXiv:astro-ph/9909275 [astro-ph].

[28] Y. Ali-Haïmoud and C. M. Hirata, Phys. Rev. D **82**, 063521 (2010), arXiv:1006.1355 [astro-ph.CO].

[29] Y. Ali-Haïmoud and C. M. Hirata, Phys. Rev. D **83**, 043513 (2011), arXiv:1011.3758 [astro-ph.CO].

[30] S. Alam et al. (BOSS), Mon. Not. Roy. Astron. Soc. **470**, 2617 (2017), arXiv:1607.03155 [astro-ph.CO].

[31] A. Chudaykin, M. M. Ivanov, and M. Simonović, (2020), arXiv:2004.10607 [astro-ph.CO].

[32] M. M. Ivanov, M. Simonović, and M. Zaldarriaga, (2019), arXiv:1912.08208 [astro-ph.CO].

[33] H. du Mas des Bourboux et al., Astron. Astrophys. **608**, A130 (2017), arXiv:1708.02225 [astro-ph.CO].

[34] M. Ata et al., Mon. Not. Roy. Astron. Soc. **473**, 4773 (2018), arXiv:1705.06373 [astro-ph.CO].

[35] W. Hu, ASP Conf. Ser. **339**, 215 (2005), arXiv:astro-ph/0407158.

[36] W. T. Hu, Wandering in the Background: A CMB Explorer, Other thesis (1995), arXiv:astro-ph/9508126.

[37] C.-P. Ma and E. Bertschinger, Astrophys. J. **455**, 7 (1995), arXiv:astro-ph/9506072 [astro-ph].

[38] D. S. Gorbunov and V. A. Rubakov, Introduction to the theory of the early universe: Cosmological perturbations and inflationary theory (2011).

[39] D. Blas, J. Lesgourgues, and T. Tram, JCAP **1107**, 034 (2011), arXiv:1104.2933 [astro-ph.CO].

[40] A. Lewis and A. Challinor, Phys. Rept. **429**, 1 (2006), arXiv:astro-ph/0601594 [astro-ph].

[41] C. Alcock and B. Paczynski, Nature **281**, 358 (1979).

[42] T. Matsubara and Y. Suto, Astrophys. J. **470**, L1 (1996), arXiv:astro-ph/9604142.

[43] W. Ballinger, J. Peacock, and A. Heavens, Mon. Not. Roy. Astron. Soc. **282**, 877 (1996), arXiv:astro-ph/9605017.

[44] X. Xu, A. J. Cuesta, N. Padmanabhan, D. J. Eisenstein, and C. K. McBride, Mon. Not. Roy. Astron. Soc. **431**, 2834 (2013), arXiv:1206.6732 [astro-ph.CO].

[45] A. Heinesen, C. Blake, Y.-Z. Li, and D. L. Wiltshire, JCAP **1903**, 003 (2019), arXiv:1811.11963 [astro-ph.CO].

[46] A. Heinesen, C. Blake, and D. L. Wiltshire, JCAP **2001**, 038 (2020), arXiv:1908.11508 [astro-ph.CO].

[47] A. L. Coil et al. (DEEP2 Survey), Astrophys. J. **609**, 525 (2004), arXiv:astro-ph/0305586 [astro-ph].

[48] M. Davis, M. J. Geller, and J. Huchra, Astrophys. J. **221**, 1 (1978).

[49] J. R. Shaw and J. Chluba, Mon. Not. Roy. Astron. Soc. **415**, 1343 (2011), arXiv:1102.3683 [astro-ph.CO].

[50] A. Drlica-Wagner et al. (DES), Astrophys. J. Suppl. **235**, 33 (2018), arXiv:1708.01531 [astro-ph.CO].

[51] A. H. Wright et al., Astron. Astrophys. **632**, A34 (2019), arXiv:1812.06077 [astro-ph.CO].

[52] M. Asgari et al., Astron. Astrophys. **634**, A127 (2020), arXiv:1910.05336 [astro-ph.CO].

[53] B. Audren, J. Lesgourgues, K. Benabed, and S. Prunet, JCAP **1302**, 001 (2013), arXiv:1210.7183 [astro-ph.CO].

[54] A. Lewis, (2019), arXiv:1910.13970 [astro-ph.IM].

[55] A. Lewis and S. Bridle, Phys. Rev. **D66**, 103511 (2002), arXiv:astro-ph/0205436 [astro-ph].

[56] A. Lewis, Phys. Rev. **D87**, 103529 (2013), arXiv:1304.4473 [astro-ph.CO].